Geophysical Journal International

Geophys. J. Int. (2012) **190,** 1169–1180 doi: 10.1111/j.1365-246X.2012.05535.x

Identification of supershear transition mechanisms due to material contrast at bimaterial faults

Sebastian Langer,[1] Louise Olsen-Kettle[1] and Dion Weatherley[1,2]

[1]*School of Earth Sciences, Earth Systems Science Computational Centre, The University of Queensland, Brisbane, Australia. E-mail: s.langer@uq.edu.au*
[2]*Sustainable Minerals Institute, WH Bryan Mining and Geology Research Centre, The University of Queensland, Brisbane, Australia*

Accepted 2012 May 3. Received 2012 April 2; in original form 2011 July 31

SUMMARY

Numerical modelling of dynamic rupture is conducted along faults separating similar and dissimilar materials. Supershear transition is enhanced in the direction of slip of the stiffer material (the negative direction) due to the bimaterial effect whereby a decrease in normal stress in front of the crack tip supports yielding ahead of the rupture. In the direction of slip of the more compliant material (the positive direction), an increase in normal stress ahead of the rupture tip delays or prevents the supershear transition, whereas the impact of the bimaterial effect on subshear ruptures is to promote rupture in the positive direction due to the tensile stress perturbation behind the rupture tip in this direction. We demonstrate that the material contrast and the parameter S control whether the transition from sub- to supershear velocity (supershear transition) is smooth or follows the Burridge–Andrews mechanism. Supershear transition along interfaces separating dissimilar materials is possible for higher values of the parameter S than supershear transition along material interfaces separating similar materials. The difference between pulse-like and crack-like rupture is small with regard to the supershear transition type.

Key words: Numerical solutions; Earthquake dynamics; Computational seismology; Wave propagation.

1 INTRODUCTION

Theoretical and experimental work have shown the existence of a transition from the Rayleigh wave speed (Rayleigh 1885) to a supershear rupture speed along homogeneous and bimaterial interfaces which is called the supershear transition. The supershear transition has also been observed along earthquake faults (Bouchon & Vallée 2003; Dunham & Archuleta 2004; Wang & Mori 2012). The possibility of rupture propagating at supershear velocities has been shown analytically by Burridge (1973). It was also shown that for a crack travelling at the Rayleigh wave velocity it is possible that the stress ahead of the crack '. . . is sufficient to overcome static friction even before the crack arrives.' (Burridge 1973). The same paper showed analytically that a crack tip can travel at the P-wave speed. However, the mechanism of a transition was not demonstrated. This was accomplished 3 yr later in numerical investigations by Andrews (1976) which led to the description of a mechanism for supershear transition along interfaces separating similar materials where a shear stress peak travelling in front of the rupture tip becomes '. . . more sharply defined and increases in amplitude' (Andrews 1976) with increasing distance from the nucleation patch. After yielding at the shear stress peak, two propagating cracks will unite and travel faster than the shear wave velocity. The rupture speed changes from subshear to supershear instantaneously. This is known as the Burridge–Andrews mechanism for supershear transitions.

The Burridge–Andrews mechanism provides a response to Eshelby's (1949, p. 310) assumption, that an admissible velocity greater than the shear wave speed would be difficult to 'connect' to from subshear velocities and that, therefore, these velocities are probably excluded in nature. Burridge *et al.* (1979) later examined the whole velocity range from below the Rayleigh wave speed to the P-wave speed. They confirmed Eshelby's (1949) claim that the range between the Rayleigh wave speed and the shear wave speed is forbidden due to the shear stress on the slip plane reversing its sign. The range between the shear wave speed and $\sqrt{2}$ of the shear wave speed is unstable due to a decease in driving load with increasing rupture velocity. Above $\sqrt{2}$ of the shear wave speed the rupture is stable. A smooth supershear transition from the Rayleigh wave speed to $\sqrt{2}$ of the shear wave speed has typically been ruled out. However, recently Festa & Vilotte (2006) and Lu *et al.* (2009) have shown in their numerical studies of homogeneous material interfaces that a smooth supershear transition is possible when an appropriate nucleation mechanism is chosen. Smooth transitioning to intersonic speeds has also been found experimentally by Singh & Shukla (1996) and Rosakis *et al.* (1998) for bimaterial interfaces. Experimental work by Xia *et al.* (2005) found smooth supershear transitions along bimaterial interfaces. The question arises: When does the supershear transition proceed as a smooth transition or as the Burridge–Andrews' mechanism along the different rupture directions? The presented

GJI Seismology

paper addresses this question for interfaces between dissimilar materials.

Ruptures propagating along bimaterial faults can generate large dynamic changes of the normal stress which influences rupture velocities and potencies differently along either the positive rupture direction (direction of slip of the more compliant material) or the negative rupture direction (direction of slip of the stiffer material). The bimaterial effect occurs for sub-Rayleigh ruptures and is a result of this change in normal stress *behind* the rupture tip. Subshear ruptures have higher rupture velocities in the positive direction due to a tensile stress perturbation *behind* the rupture tip which continues forward after the rupture front has moved on and promotes rupture in this direction (Weertman 1980; Andrews & Ben-Zion 1997; Rubin & Ampuero 2007) with higher potencies and a preference for this direction in case of unilateral rupture (Ben-Zion 2001; Ampuero & Ben-Zion 2008; Langer *et al.* 2010). Conversely, in the negative direction, the sign of the normal stress change is reversed and the normal stress change is compressive *behind* the rupture tip leading to dynamic strengthening and lower rupture velocities for subshear rupture. The bimaterial effect is relatively well known and studied; however, here we examine another effect which arises in bimaterial interfaces: the normal stress changes in *front* of the rupture tip which influence whether or not a supershear transition will occur. The supershear transition is enhanced in the negative direction, where normal stress changes ahead of the rupture unclamp the fault, making it easier for the shear wave stress peak to trigger supershear failure of the fault. The opposite applies in the positive direction, such that the transition is delayed or sometimes even suppressed.

Harris & Day (1997) have shown the existence of supershear rupture in the negative direction in numerical simulations. Their highest rupture velocity is close to the primary wave speed of the slower material. Ranjith & Rice (2001) and Adams (2001) provide analytical evidence for supershear ruptures exclusively in the negative direction. However, the authors do not mention a transition to supershear velocities, they rather state the possible existence of supershear ruptures in the negative direction in general. In numerical investigations, Shi & Ben-Zion (2006) use a nucleation patch which expands at the primary wave speed of the slower material to nucleate rupture and, thereupon, observe supershear speeds in both directions. This paper investigates if a supershear transition along a bimaterial interface can be observed and if it follows the Burridge–Andrews mechanism. So far a transition to supershear along a bimaterial interface has only been shown in experimental work by Xia *et al.* (2005) as a smooth transition for a Homalite-100/Polycarbonate interface. We provide a step-by-step explanation of the supershear transition mechanisms present at bimaterial interfaces similar to the one provided for the homogeneous case by Andrews (1976).

A numerical model is presented here capable of producing the Burridge–Andrews mechanism as well as a smooth supershear transition along bimaterial interfaces for crack-like as well as pulse-like ruptures. The paper highlights the dependence of the transition mechanism on the material contrast at the interface and on the upper yield point parameter S[1] given by (Andrews 1976, here called 'parameter S'). The paper also explains the occurrence of the Burridge–Andrews mechanism in Xia *et al.* (2004) along an interface separating similar materials in contrast to a smooth transition along a bimaterial interface in Xia *et al.* (2005).

[1] In other work, this parameter is called strength excess parameter (Ampuero & Ben-Zion 2008); actual fault strength with respect to the released stress (Festa & Vilotte 2006); measure of material strength relative to tectonic stress (Das & Aki 1977); dimensionless parameter (Harris & Day 1993); seismic ratio (Dunham 2007; Lu *et al.* 2009) or non-dimensional driving stress parameter (Xia 2005).

2 NUMERICAL MODEL

Numerical solutions of dynamic fault rupture are studied using the finite element method (FEM) implemented in the ESYS.ESCRIPT software (Gross *et al.* 2007). A numerical simulation consists of two phases, first a quasi-static loading phase to apply compressive and shear stresses to the model and secondly a dynamic phase where rupture is initiated and observed.

In the quasi-static loading phase, numerical solutions of the static elastic deformation equation $\sigma_{ij,j} = 0$ are obtained as in Langer *et al.* (2010). In all simulations, a far-field normal stress σ_N and a far-field shear stress τ are applied to the model, as shown in Fig. 1. The bimaterial studies are conducted using periodic boundaries (dashed lines) to prevent stress distortions along the fault face as in Langer *et al.* (2011). The acquired stress field provides the initial conditions for the dynamic rupture phase.

A triangular mesh is constructed using Gmsh (Geuzaine & Remacle 2009). It consists of triangles and is 950 mm × 350 mm wide. To model a 600-mm-long fault Γ during the dynamic rupture phase, contact joint elements are used in the same fashion as in Langer *et al.* (2010) and Olsen-Kettle *et al.* (2008), which is similar to the traction-at-split-node method used by Duan & Oglesby (2005), Andrews (1999), Day *et al.* (2005) and Rojas *et al.* (2008). Numerical solutions of the 2-D wave equation are studied where the penalty method is used to enforce the contact boundary conditions as in Perić & Owen (1992), Laursen & Simo (1993) and Wriggers (2006).

As in Langer *et al.* (2011) a velocity weakening friction law by Ampuero & Ben-Zion (2008) is used with the ability to model pulse-like as well as crack-like rupture. The friction coefficient along the

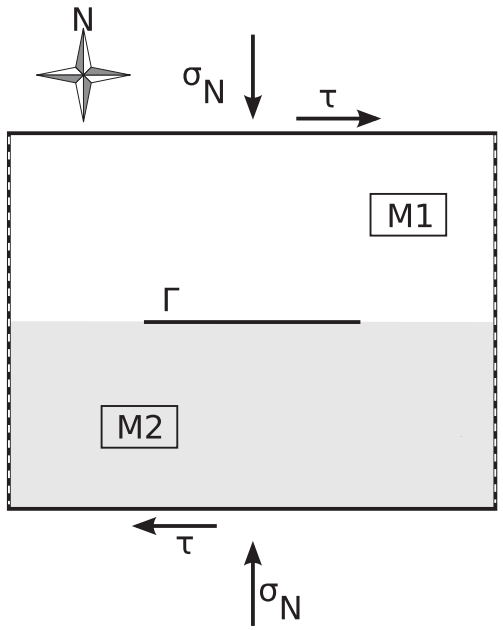

Figure 1. This model is used for numerical simulations with periodic boundary conditions. The dashed parts of the model boundary have periodic properties. The model has a size of 950 mm × 350 mm with a central fault Γ 600 mm long.

fault is defined as

$$\mu_f = \mu_s + \alpha \frac{V}{V + V_c} - \beta \frac{\Theta}{\Theta + V_c}, \quad (1)$$

where V is the plastic slip-rate, μ_s is the static friction coefficient and α quantifies a rate (as in rate and state dependent friction laws) on the currently acting friction μ_f. The evolution effect β is a direct velocity strengthening mechanism with a regularizing effect (Ampuero & Ben-Zion 2008). The dynamic friction coefficient can be calculated as $\mu_d = \mu_s + \alpha - \beta$. V_c is a characteristic velocity scale and τ_c is a characteristic timescale governing the evolution of the state variable Θ through

$$\dot{\Theta} = \frac{V - \Theta}{\tau_c}. \quad (2)$$

Throughout the simulations a constant characteristic slip-weakening distance $D_c \doteq V_c \tau_c$ is maintained. Whenever V_c is varied, τ_c changes accordingly. Lower values of V_c lead to crack-like ruptures whereas higher values yield pulse-like rupture as in Ampuero & Ben-Zion (2008) and Langer *et al.* (2011). During simulations it was determined if ruptures are pulse-like or crack-like. This was done separately for the positive and the negative direction. A rupture is called crack-like if, when the rupture reaches the end of the fault Γ, there is no fault segment between the nucleation patch and fault end where rupture has ceased. Otherwise the rupture is pulse-like.

Supershear transitions are expected to either be smooth with a crack tip that immediately accelerates to supershear velocity as in Xia *et al.* (2005) or to follow the Burridge–Andrews mechanism. When the Burridge–Andrews mechanism is present, for a small number of time steps there will be two cracks along the fault which are not connected: the original crack and the daughter crack which is caused by the yielding shear stress peak. They will eventually unite and propagate at supershear velocities as one crack. To identify which transition type is present during ruptures the number of cracks is observed. If there are two cracks and if the rupture speed after the occurrence of the two cracks is equal to or higher than the lower shear wave speed of the involved materials then a Burridge–Andrews mechanism is assumed. The unslipped fault segment between the two cracks is called the transition gap and its length is the transition gap width. If supershear velocity is reached without the occurrence of two cracks at any past time of the rupture, the transition is smooth and the transition gap width is equal to zero. The transition length is the distance between nucleation patch and the location at fault where the supershear transition occurs and is assumed to depend on stresses acting on the fault as well as frictional and material properties as discussed in Xia *et al.* (2004), Rosakis *et al.* (2007) or Mello *et al.* (2010).

As a necessity for numerical stability the mesh grid step size Δx has to be smaller than the lower limit of the quasi-static length scale λ_{cr}, which for the mesh presented here is calculated for a Polycarbonate/Homalite-100 pair according to Ampuero & Ben-Zion (2008) as

$$\lambda_{cr} \approx \frac{\pi \mu' D_c}{(\beta - \alpha)\sigma} \frac{1}{\sqrt{1 + \left(V_c / V_{dyn}\right)^2}} = 0.066 \text{ m} \quad (3)$$

with

$$V_{dyn} = \frac{(\beta - \alpha)\sigma}{\mu'/2c_R} \sqrt{\frac{\alpha}{\beta - \alpha}} \quad (4)$$

and $\mu' = 2.2$GPa is the effective elastic modulus determined as in Rubin & Ampuero (2007).[2] A mesh consisting of triangles with a grid step size of $\Delta x = 0.001$m along the fault and everywhere within the domain is used to observe the dynamic rupture propagation within the continuum limit. The values for Δx are chosen to be so small in an attempt to obtain a good resolution of the Burridge–Andrews mechanism.

It has been found by Renardy (1992) that the sliding of an elastic solid against a rigid body causes short-wavelength perturbations near the interface. Ranjith & Rice (2001) showed analytically that for a material pair with dissimilar elastic moduli with an existing generalized Rayleigh wave speed the sliding is ill-posed. They propose regularization of the ill-posedness by introducing a fading memory to the normal stress. The numerical framework used in this paper is derived from the source code by Olsen-Kettle *et al.* (2008) and incorporates an inherent general memory effect through the elastic response of the fault. An elastic predictor, using a first-order Taylor expansion, estimates the Coulomb failure stress at a future time step by assuming first that at this time step the incremental displacement is purely elastic along the fault. If the estimated elastic failure stress is larger than zero, plastic yielding in the current time step is initiated and calculated so that the Coulomb failure stress at the next time step remains on the yield surface. This prevents physically invalid positive values of Coulomb failure stress. Since only the plastic slip-rate and not the total slip-rate is used in our friction law (see eq. 1), the elastic component of the slip may provide a memory dependence through the elastic fault response. Olsen-Kettle *et al.* (2008) showed, that this greatly reduces the mesh-dependency associated with the ill-posedness in the sense of Renardy (1992). Ampuero & Ben-Zion (2008) deployed the regularization mechanism by Rubin & Ampuero (2007) for the friction law used here. In Section 5, simulations with this regularization mechanism are conducted to highlight the influence of the delay of normal stress response.

Nucleation conditions are known to influence rupture mode and supershear transition as shown in Festa & Vilotte (2006), Shi *et al.* (2008) and Lu *et al.* (2009). Ampuero & Ben-Zion (2008) used a simple nucleation procedure to minimize the number of arbitrary assumptions about the nucleation. They were able to observe a wide range of rupture phenomena. For the simulations presented here rupture is nucleated by setting the static friction in the nucleation site to a value of $\mu_s = |\tau|/|\sigma_N| - 0.001$ as in Langer *et al.* (2011) and in a similar way to Ampuero & Ben-Zion (2008). During the loading phase the fault is still welded together by an infinitely high cohesion. To nucleate dynamic rupture, the cohesion is lowered to zero along the fault. In the nucleation patch μ_s is set to the lowered static friction value throughout the simulation. An overview of model parameters is shown in Table 1. The size of the nucleation patch is 11mm. It is centred about the midpoint of the fault.

3 SUPERSHEAR TRANSITION ALONG HOMOGENEOUS INTERFACES

Initially a fault separating similar materials is studied to compare the supershear mechanism with previous work and to establish a reference for bimaterial experiments. More than 1500 simulations were conducted using eight cores each of an SGI ICE 8200 EX Parallel Computer at 2.8 GHz. Each simulation takes on average 90 min. The materials used in the simulations are Homalite-100 as in

[2] Note, that Ampuero & Ben-Zion (2008) show a homogeneous case in their eqs (A4) and (A6) with μ' replaced by $\mu/(1 - \nu)$.

Table 1. Simulation parameters used in this study.

Description	Parameter	Value
Mesh dimensions	(m), (m)	0.95, 0.35
Fault length	Γ (m)	0.6
Maximum mesh grid step size	Δx (m)	0.002
Background normal stress across interface	σ_N (MPa)	-11.6
Background tangential stress along interface	τ (MPa)	4.0
Direct effect coefficient	α	0.001
Evolution effect coefficient	β	0.401
Stress drop	f_s	0.4
Slip-weakening distance	D_c (m)	1×10^{-5}

Table 2. Material properties according to Xia *et al.* (2005).

Description	Parameter	Homalite-100	Polycarbonate
Rigidity modulus	μ (GPa)	1.8	1.1
Lamé's first parameter	λ (GPa)	4.2	3.5
Poisson's ratio	ν	0.35	0.38
Density	ρ (g cm^{-3})	1.262	1.192
Rayleigh wave velocity	C_R (m s^{-1})	1122	902
Shear wave velocity	C_S (m s^{-1})	1200	960
Primary wave velocity	C_P (m s^{-1})	2498	2182

Xia *et al.* (2004) and Polycarbonate which together with Homalite-100 has been used in Xia *et al.* (2005). Material properties are shown in Table 2.

A range of the parameter S and the characteristic timescale V_c of the friction law are used to obtain pulse-like as well as crack-like ruptures for different fault strengths. To be able to compare results, the same applied stresses σ_N, τ and stress drop $f_s = \mu_s - \mu_d$ are maintained for all simulations. For the material Homalite-100, Xia (2005, p. 50) experimentally identified $f_s = 0.4$. The supershear transition occurs more readily for lower values of S according to Andrews (1976) and Das & Aki (1977). The parameter S can be calculated as

$$S = \frac{\mu_s |\sigma_N| - |\tau|}{|\tau| - \mu_d |\sigma_N|} = \frac{(\mu_d + f_s)|\sigma_N| - |\tau|}{|\tau| - \mu_d |\sigma_N|}. \quad (5)$$

Eq. (5) can be rearranged to obtain μ_s and μ_d for a desired S

$$\mu_d = \frac{|\tau|}{|\sigma_N|} - \frac{f_s}{S+1}$$
$$\mu_s = \mu_d + f_s. \quad (6)$$

In simulations of fault rupture for a range of V_c and S the transition gap widths are recorded and shown in Fig. 2. The phase diagrams show transition gap widths as the number of integration points along the fault that have yet to slip. The transition gap width increases with the parameter S. Burridge (1973, p. 448) assumed that the shear stress peak travels at the shear wave speed from the moment of nucleation. As the crack tip travels at below or at the Rayleigh wave speed, the distance between the crack tip and shear stress peak increases with distance from nucleation patch. Andrews (1976, Figs 4 and 5) showed an increasing transition gap width as well. Festa & Vilotte (2006) observed the peak travelling at the shear wave speed. If the supershear transition occurs close to the nucleation site, there is no distinction between the crack tip and the shear stress peak and the transition appears to be smooth. It is called here the unresolved supershear transition mechanism and appears as in Fig. 2 for lower parameters S.

The significance of the transition gap width lies in its relation to the supershear transition length. If the transition length is very short, so that the transition gap width is smaller than one element size, it can not be excluded that the Burridge–Andrews mechanism is acting, even though it is not observable. For larger transition lengths a non-existent transition gap width can not be attributed to coarse grid step sizes and has to be caused by a genuine smooth transition mechanism. The minimum rupture time of the shear wave from the nucleation point to observe the Burridge–Andrews mechanism for a given mesh resolution can be determined by solving the equation

$$V_S t - V_R t = \Delta x \quad (7)$$

for the rupture time t where V_R and V_S are the Rayleigh speed and shear wave speed, respectively. The grid step size in the simulations conducted here must be smaller than the smallest observable transition gap. The minimal distance d from the nucleation patch with a separately yielding shear stress peak is thus

$$d = \frac{\Delta x}{V_S - V_R} V_S. \quad (8)$$

The simulations for Homalite-100 in Fig. 2(b) have been repeated for mesh sizes two and four times smaller. By noting the shortest transition length for each grid step size within the number of conducted simulations, we found that indeed the minimum existing transition time for the Burridge–Andrews mechanism and its transition gap width observable in our simulations decreased for smaller grid step sizes. For $\Delta x = 1000$ µm, $\Delta x = 500$ µm and $\Delta x = 250$ µm the minimum transition times were 47, 38 and 34 µs and minimum transition lengths were 28, 22 and 18 mm, respectively.

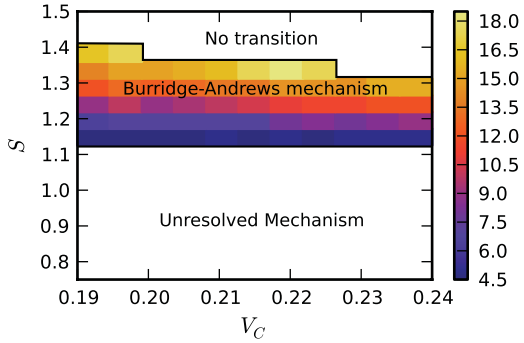

(a) Transition gap width for Polycarbonate in millimeters

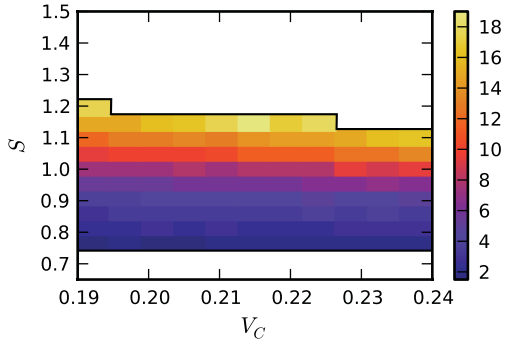

(b) Transition gap width for Homalite-100 in millimeters

Figure 2. The graphs show the distance between the crack tip and the shear stress peak (transition gap) at the time of supershear transition in millimetres along the fault. For low values of parameter S the transition is seemingly smooth as the Burridge–Andrews mechanism is not resolved. For high values of S, there is no transition within the half length of the fault. The velocity length scale V_c of the friction law controls the rupture mode with $V_c = 0.19\,\mathrm{m\,s^{-1}}$ yielding crack-like rupture and $V_c = 0.24 m\,s^{-1}$ yielding pulse-like rupture.

The unresolved and apparently smooth transition described here is different from Lu *et al.* (2009) where they observe a distinct shear stress peak, but the transition occurs at the original crack tip. In their simulations, the nucleation mechanism is responsible for either smooth transitioning or the Burridge–Andrews mechanism. The work presented here is also different from Festa & Vilotte (2006) where for their cases a distinct shear stress peak exists.

With increasing S the transition length increases and the Burridge–Andrews mechanism can be observed. For cases with $S \gtrsim 1.4$ (Polycarbonate) and $S \gtrsim 1.2$ (Homalite-100) the supershear transition length rises beyond the fault half length and no transition occurs. Fig. 2 shows the existence of the Burridge–Andrews mechanism for both pulse-like and crack-like rupture where the distance between the crack tip and shear stress peak is larger than zero.

In preparation for showing the smooth transition mechanism along bimaterial interfaces the Burridge–Andrews mechanism is shown in the same way as by Andrews (1976). Andrews uses the dimensionless stress change

$$Z = \frac{\left|\sigma_{xy}\right| - |\tau|}{|\tau| - \mu_d \left|\sigma_{\mathrm{N}}\right|}, \tag{9}$$

to show the difference between the current shear stress σ_{xy} and the background shear stress along the fault. This difference in the numerator is then normalized by the final stress drop in the denominator. In Fig. 3, the graphs show the transition mechanism for times before, during and after the transition to supershear rupture speeds for a crack-like rupture by plotting the dimensionless stress change and plastic slip. The figures are consistent with and very similar to Andrews (1976). We also present plots of shear stress, normal stress and Coulomb failure stress which will be important when studying simulations with material dissimilarities across the fault where reduction of normal stresses is reflected in the Coulomb failure criterion and helps to explain bimaterial supershear transitions.

4 SUPERSHEAR TRANSITION ALONG BIMATERIAL INTERFACES

In nature faults often separate dissimilar materials. Smooth supershear transitions were shown to be possible in the negative direction in laboratory experiments by Xia *et al.* (2005). To shed light on the mechanism of such a smooth transition and to determine its dependence on material contrast simulations of rupture along bimaterial interfaces were conducted. As Xia *et al.* (2004) found a Burridge–Andrews mechanism for a homogeneous material interface and smooth transitions for a bimaterial Polycarbonate/Homalite-100 interface in Xia *et al.* (2005), simulations with a wide range of material contrast are conducted to investigate both cases. The material pairs consist of a more compliant material M2 (see Fig. 1) and a stiffer material M1, where the material properties are set by manipulating the contrast parameter k

$$\begin{aligned} \rho_{M1} &= \frac{1-k}{2}\rho_{\mathrm{P}} + \frac{1+k}{2}\rho_{\mathrm{H}} \\ P_{M1} &= \frac{1-k}{2}P_{\mathrm{P}} + \frac{1+k}{2}P_{\mathrm{H}}\,, \\ S_{M1} &= \frac{1-k}{2}S_{\mathrm{P}} + \frac{1+k}{2}S_{\mathrm{H}}, \end{aligned} \tag{10}$$

where P_{H}, P_{P}, S_{H}, S_{P}, ρ_{H} and ρ_{P} are the primary wave speed, the shear wave speed and the density of Polycarbonate and Homalite-100, respectively. To obtain the values for M2, the signs before the k's in eq. 10 simply have to be negated. For $k = 0$ the same material with the wave speeds and density as the average of Homalite-100 and Polycarbonate will be calculated. A contrast $k = 1$ results in the moduli for Polycarbonate as the more compliant and Homalite-100 as the stiffer material. A generalized Rayleigh wave speed in the sense of Weertman (1963) (not as in Stoneley (1924) for 'welded' interfaces) exists for the bimaterial pairs in the parameter sweeps, except for the values at $k = 1.1$. The maximum contrast for which a generalized Rayleigh wave speed exists is $k = 1.061$ when the Rayleigh wave speed is calculated according to Weertman (1963, eq. 15) with a spelling correction for his variable γ where the square root over the term is missing.

To explain the conditions for a smooth supershear transition, the transition mechanism is shown in Fig. 4 for a material pair with particularly high contrast $k = 1$ and a high value of the parameter $S = 1.15$. For the chosen parameter pair a smooth transition is present; however, for slightly lower values of k the transition would follow the Burridge-Andrews mechanism. This demonstrates best how the effect of the material contrast alters the Burridge–Andrews mechanism to result in a smooth transition. Fig. 4 shows the normal, shear and Coulomb failure stress during a smooth transition.

In the negative direction normal stress reduction is observed in front of the crack at time step $\Delta t = 27\mu$s. Behind the crack tip the compressive stress is higher than the background compression. The shear stress peak in front of the crack tip looks similar to the homogeneous case and increases in amplitude. However, as the normal stress in front of the crack tip is reduced, it promotes yielding. The time step $\Delta t = 37\mu$s shows the peak in the yield criterion nearly disappearing in the negative direction. The shear stress peak is still observable and as it rises further it also interacts with the normal stress in front of the crack tip which leads to smoothing and elevating of the local minimum in shear stress peak and crack tip. This is the important difference to the Burridge–Andrews mechanism. The peak shear stress and the crack tip unite before the yield criterion is met at the shear stress peak. This can be seen at time step $\Delta t = 61\mu$s. In agreement with Weertman (2002) and Shi & Ben-Zion (2006) the normal stress change is dilational behind the crack tip after the supershear transition has occurred in the negative direction at time step $\Delta t = 71\mu$s. It can also be derived from these plots that the normal stress reduction leads to a shorter nucleation distance as the yield criterion in front of the crack tip is met earlier than it would have been for a homogeneous material.

In the positive direction, smooth transitions are not observed. As time step $\Delta t = 27\mu$s in Fig. 4 shows, the bimaterial effect causes higher normal stresses in front of the crack tip and extensional stresses behind the the crack tip similar to Andrews & Ben-Zion (1997, Fig. 7). The bimaterial effect becomes more pronounced with distance from the nucleation patch as described in Ranjith & Rice (2001). As can be seen in the subsequent time steps, the normal stress concentration prevents a uniting of shear stress peak and crack tip and decreases the Coulomb failure stress which then prevents either of the supershear transition mechanisms.

With the explanation for a smooth transition mechanism at hand, a parameter study would be useful to explore the dependence of the mechanism on the characteristic velocity scale V_{c}, the parameter S and the material contrast k. However, this would be computationally expensive. Fig. 2 shows for a rupture along a homogeneous material interface that all transition types occur for a wide range of V_{c} and that thus the influence of V_{c} on the transition mechanism is small compared to the influence of S. Therefore, only two parameter sweeps for $V_{\mathrm{c}} = 0.19\,\mathrm{m\,s^{-1}}$ (crack-like rupture) and $V_{\mathrm{c}} = 0.24\,\mathrm{m\,s^{-1}}$ (pulse-like rupture) over S and k are conducted. Fig. 5

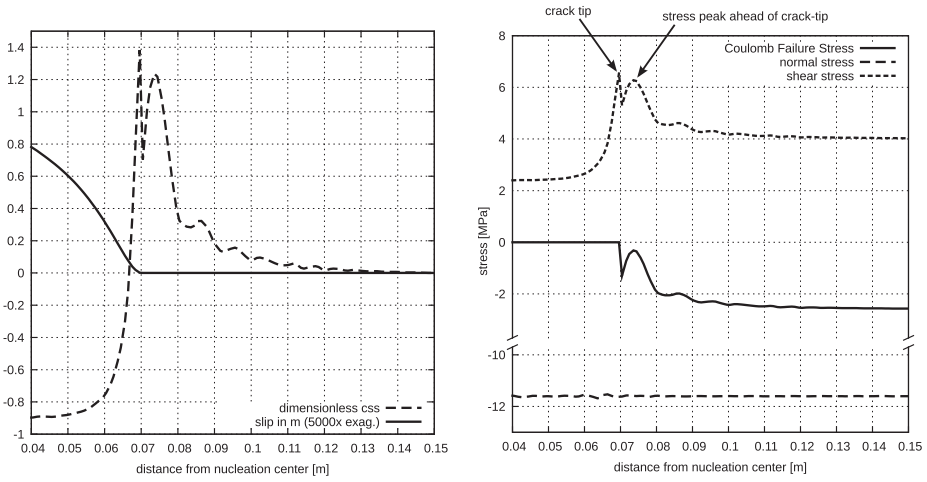

(a) $T = 70\,\mu$s, before transition

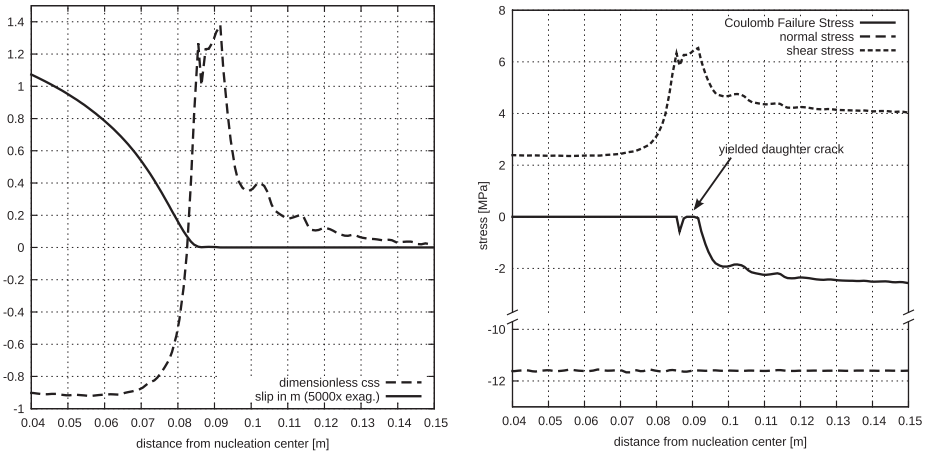

(b) $T = 86\,\mu$s, during transition

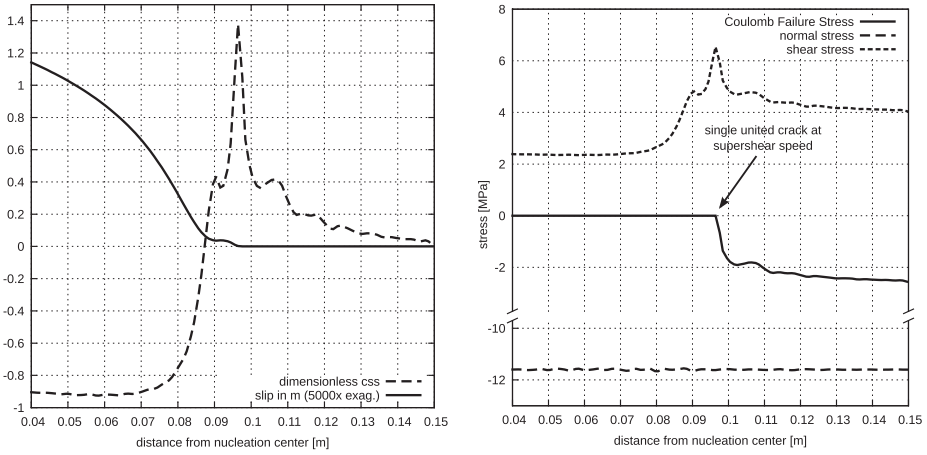

(c) $T = 90\,\mu$s, after transition

Figure 3. Supershear transition along a homogeneous interface through the Burridge–Andrews mechanism described in Andrews (1976). The figures show the normal and shear stresses and the resulting Coulomb failure stress along the fault before, during and after the supershear transition on the right-hand side. On the left-hand side, the plastic slip and the dimensionless change of shear stress (dimensionless css) are shown in the same manner as by Andrews (1976).

shows the resulting phase diagrams for pulse-like and crack-like rupture.

Fig. 5(a) shows the transition mechanism dependence on the parameter S and the material contrast k for the negative direction. The circled numbers in the Figure mark regions of interest. Region (1) shows the Burridge–Andrews mechanism for a homogeneous or low-contrast material with a parameter S which leads to supershear rupture at a longer transition length. It occurs more readily

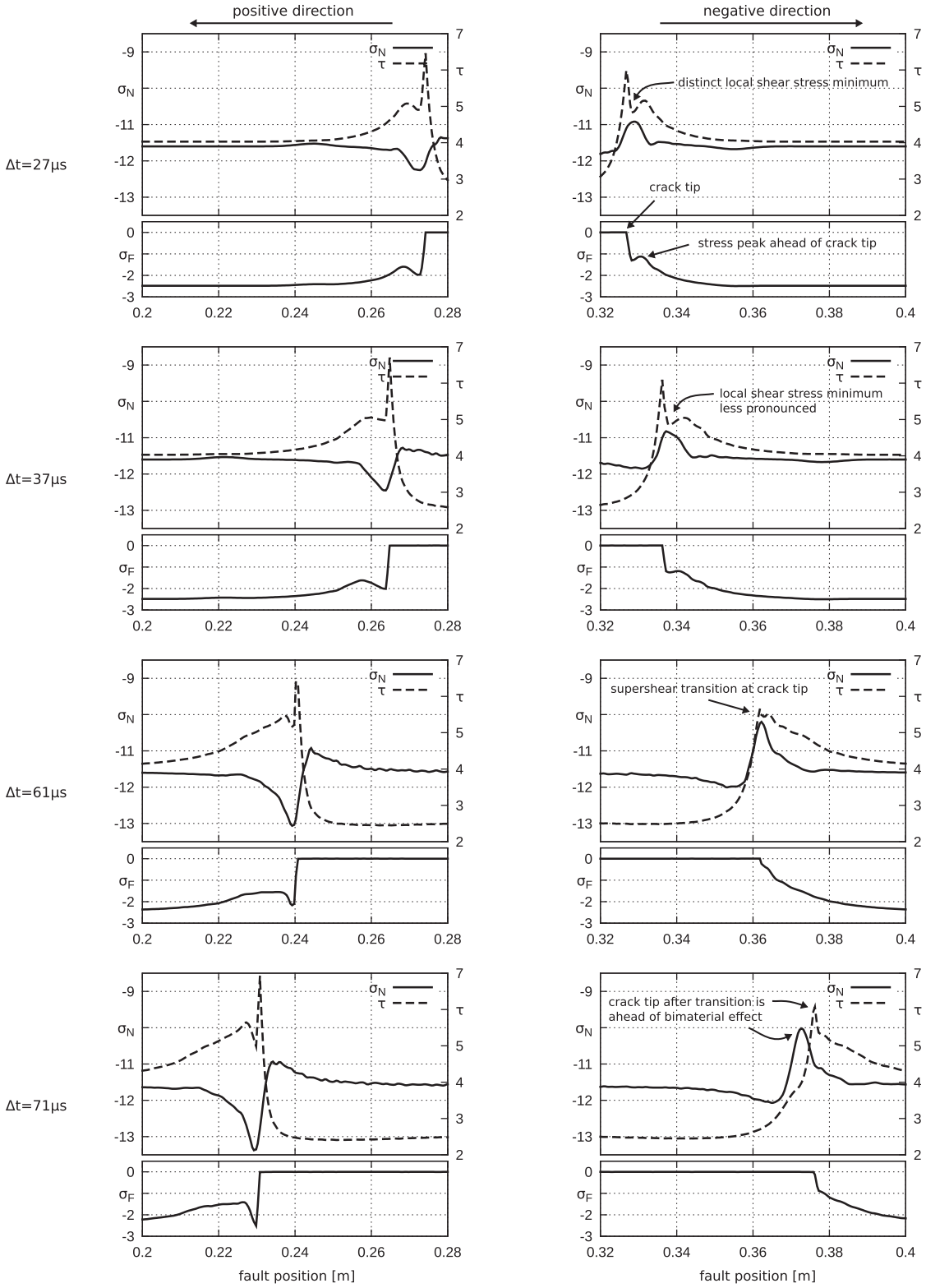

Figure 4. A supershear transition along a bimaterial interface is shown for the negative direction (the direction of slip of the stiffer material). In the negative direction, the transition occurs smoothly at $\Delta t \approx 61\,\mu s$. In the positive direction no supershear transition occurs. The normal stress σ_N, the shear stress τ and the Coulomb failure stress σ_F across the fault are shown in MPa.

for lower material contrast as the bimaterial effect is not as strong. Region (2) shows the unresolved transition mechanism caused by the short transition length as in the homogeneous case in Fig. 2. In region (3) the bimaterial effect is strong due to the high material contrast and leads to the smooth transition described in Fig. 4. It is interesting to see that with lower values of the parameter S the smooth supershear transition occurs for lower material contrasts. The reason is that for lower S, the transition length and the

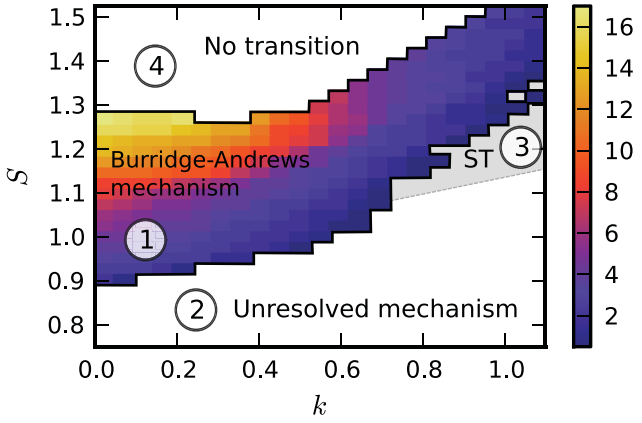

(a) Transition gap width in millimeters for crack-like rupture in the negative direction (ST stands for smooth transition)

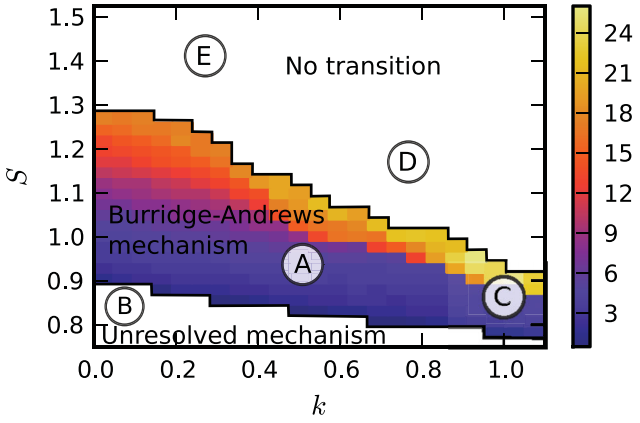

(b) Transition gap width in millimeters for crack-like rupture in the positive direction

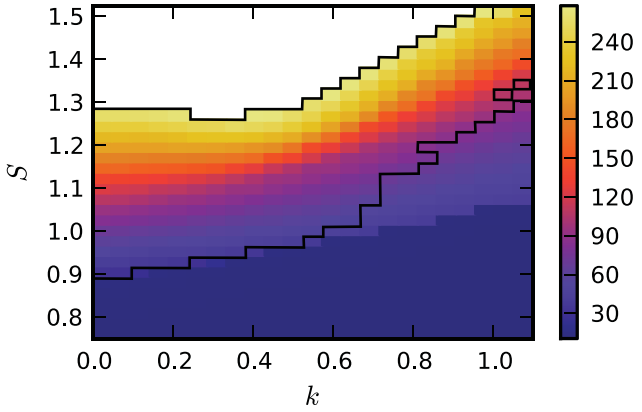

(c) Transition length in millimeters for crack-like rupture in the negative direction

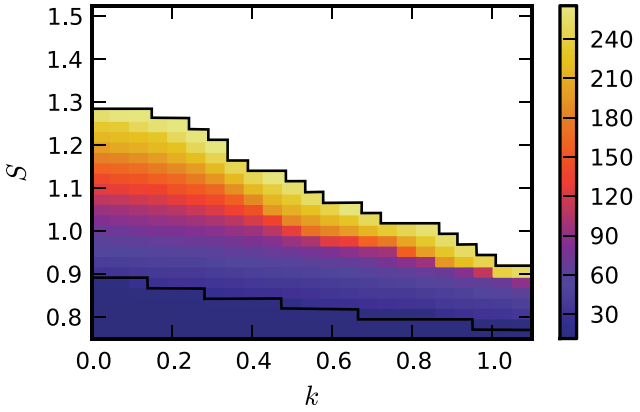

(d) Transition length in millimeters for crack-like rupture in the positive direction

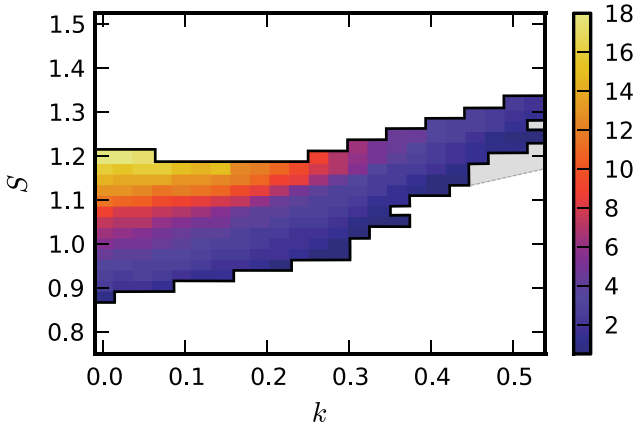

(e) Transition gap width in millimeters for pulse-like rupture in the negative direction

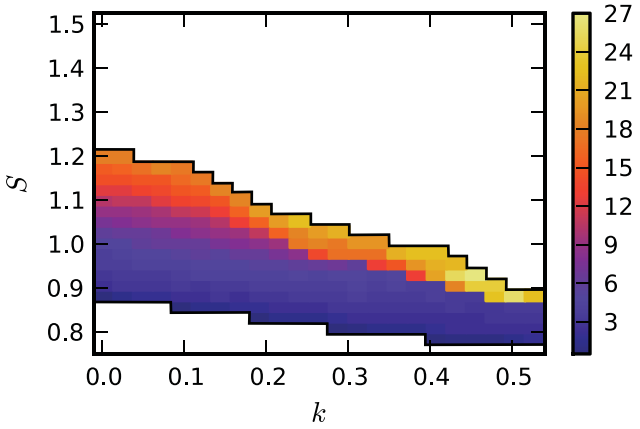

(f) Transition gap width in millimeters for pulse-like rupture in the positive direction

Figure 5. The phase diagrams show rupture modes in the positive and the negative direction for different fault strengths S and different material contrasts defined by k. The smooth transition only exists for the negative direction and the Burridge–Andrews mechanism exists for both directions up to a certain material contrast. Panels (c) and (d) show the transition length for the supershear transitions in panels (a) and (b), where the black lines shows the border between the transition mechanisms in the parameter sweeps.

transition gap are smaller and it is easier for the tensile normal stress change in front of the crack tip in the negative direction to smear these differences out and promote a smooth transition. Region (4) has high values of parameter S which means that supershear transition will not occur within the length of the fault or at all (see Burridge 1973, eq. 4.12) for a distinction between these two cases for ruptures along similar materials). However, for the same parameter S a higher material contrast as in region (5) causes a supershear transition, smooth as well as the Burridge–Andrews mechanism. The reason is that in the negative direction the bimaterial effect generally brings the fault closer to yielding in front of the crack tip by reducing normal stress. Whether the Burridge–Andrews mechanism or a smooth transition occurs depends on how strong the bimaterial effect is compared to normal strength at the fault. For a strong bimaterial effect the transition gap gets smaller even though the transition length (see Fig. 5c) remains high. This is caused by the bimaterial effect 'elevating' the shear stress minimum within the transition gap. If the lifting is partial by the time yielding at the shear stress peak is reached, the transition gap is smaller. For a subset of cases with $k \gtrsim 0.8$ and $S \gtrsim 1.1$ a smoothing suppressing the local minimum at large transition lengths is observed which leads to the formerly described smooth transition at time step $\Delta t = 61\,\mu$s in Fig. 4.

In the positive direction, a supershear transition is less favoured as can be seen in Fig. 4. However, the bimaterial effect is not strong for low material contrasts, so a Burridge–Andrews mechanism is evident in region (A) in Fig. 5(b). Region (B) shows an unresolved transition mechanism for low S as in Fig. 2 for the homogeneous cases of Polycarbonate and Homalite-100 or region (2) in the negative direction. Region (C) has a Burridge–Andrews mechanism for lower values of S and higher material contrasts. In these cases, the bimaterial effect extends the transition length. The transition gap width rises when the crack tip distances itself from the nucleation patch. When the transition occurs, the transition gap width is large enough to cause a Burridge–Andrews mechanism. From Fig. 5(d) it can be observed that the compressive normal stress in front of the crack tip causes the transition length to increase which results in high transition gaps for medium values of the parameters S in Fig. 5(b). Region (D) shows that for higher S and higher material contrast k, the normal stress change prevents supershear rupture in the positive direction, an effect known from numerous papers (Cochard & Rice 2000; Adams 2001; Ranjith & Rice 2001; Shi & Ben-Zion 2006). In region (E) no transition occurs within the length of the nucleation patch due to a high value of S.

When analysing the Figs 5(a)–(d), we can identify the rupture profile shown in the experimental results of Xia *et al.* (2005, case 3) which can be seen in regions (3) & (E) for higher S. In this region there is a smooth transition in the negative direction and no transition in the positive direction. Regions (3) & (D) correspond to Xia *et al.* (2005)'s case 2 with a very short transition length in the negative direction and no supershear transition in the positive direction. Figs 5(e) and (f) show that for pulse-like rupture the same phenomena occur as for crack-like rupture. The results explain the occurrence of immediate supershear rupture and supershear transition in the negative direction in the experiments by Xia *et al.* (2005).

Mesh dependency tests at two and four times finer than the originally used mesh size for simulations with material contrasts are shown in Table 3 for simulations with and without supershear transition. These results show convergence of our numerical method with grid size reduction.

Table 3. Grid step-size dependency for supershear transitions in the negative direction for a crack-like rupture ($V_c = 0.19\,\mathrm{m\,s^{-1}}$).

	Before transition			Rupture at fault end	
Grid step size Δx (μm)	Rupture speed $V_R c_{GR}^{-1}$	Average slip (μm)	Transition length (mm)	Rupture speed $V_R P_{M1}^{-1}$	Average slip (μm)
No supershear transition ($S = 1.35, k = 0.5$)					
1000	1.01	182			
500	0.99	175		No transition	
250	0.99	170			
Supershear transition ($S = 1, k = 0.25$)					
1000	1.03	60.0	60	0.86	205
500	0.99	91.7	88	0.86	205
250	0.99	113	108	0.86	205

5 REGULARIZATION OF NORMAL STRESSES

The ill-posedness of sliding of two dissimilar materials with an existing generalized Rayleigh wave speed has been shown by Ranjith & Rice (2001). The simulations in Sections 3 and 4 are conducted using the elastoplastic fault model proposed by Olsen-Kettle *et al.* (2008) where they showed that ill-posedness is marginal through the incorporation of both an elastic ('memory' dependent) and plastic (instantaneous slip) fault response. The plastic slip is calculated by ensuring that the Coulomb failure stress is met at all time steps. Cochard & Rice (2000) discuss the numerical problems of Andrews & Ben-Zion (1997) and show, that with regularization the numerical solutions of the dynamic rupture propagation do not show ill-posedness. In this section, we examine how an additional regularization affects the occurrence of the different supershear transition mechanisms. Ranjith & Rice (2001) propose regularization of the ill-posedness by introducing a fading memory to the normal stress. Rubin & Ampuero (2007) and Ampuero & Ben-Zion (2008) used the spectral boundary integration element method by Cochard & Rice (2000) and applied a method where regularization delays the normal stress response

$$\dot{\sigma^*} = \frac{V^*}{\delta_\sigma}\left(\sigma - \sigma^*\right). \tag{11}$$

In Fig. 6, the transition gap width in regularized and non-regularized simulations are compared for crack-like rupture. Parameters are defined as in Ampuero & Ben-Zion (2008) with $V^* = 2m\,s^{-1}$ and $\delta_\sigma = 0.95\,D_c$. As described by Ampuero & Ben-Zion (2008), the bimaterial effects becomes delayed and less pronounced in amplitude. The Burridge–Andrews mechanism occurs for a wider portion of the phase diagram than for non-regularized cases. As the bimaterial effect is dampened by the evolution law in eq. (11) the effective extensional stress change in front of the crack tip is shifted past the crack tip and has a weaker interaction with the shear stress peak in front of the rupture tip. Fig. 6 shows the transition mechanisms in comparison with the non-regularized case. For the negative direction (Fig. 6a) the Burridge–Andrews mechanism appears for higher material contrasts than in the non-regularized simulations.

In non-regularized simulations transition lengths for low values of parameter S are short and supershear transition is smooth as the crack tip and shear stress peak have not yet separated. An increasing material contrast prevents short transition lengths in the positive direction and leads to the Burridge–Andrews type supershear mechanism. When regularization is used the bimaterial effect is weakened and transition lengths are shorter than in the non-regularized simulations. This leads to a more frequent occurrence

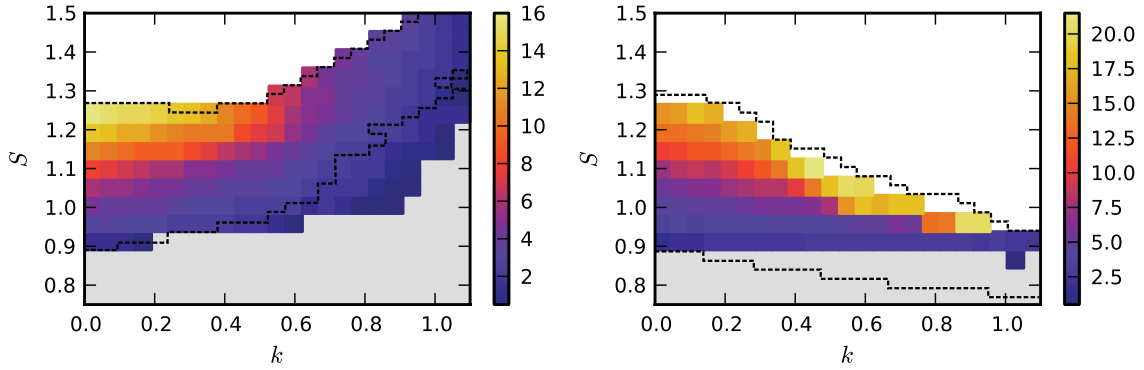

(a) Transition gap width in millimeters for regularized crack-like rupture in the negative direction

(b) Transition gap width in millimeters for regularized crack-like rupture in the positive direction

Figure 6. Regularizing the ill-posedness of dissimilar materials against each other shows a shift in transition mechanism. The dashed lines show the boundaries between transition mechanism for the non-regularized phase diagrams 5(a) and 5(b) for comparison. The grey region shows smooth transitions, the colours show the transition gap widths for the Burridge–Andrews mechanism and the white region shows parameter pairs where no transition occurs.

of Burridge–Andrews mechanisms in the regularized than in the non-regularized simulations for higher material contrast and low parameter S in the direction of slip of the more compliant material.

6 DISCUSSION

This work numerically explores supershear transitions along bimaterial interfaces. It focuses on the influence of the parameter S (Andrews 1976) and the material contrast on the supershear transition mechanism. Two different types of supershear transition mechanisms have been found: the Burridge–Andrews mechanism (Burridge 1973; Andrews 1976) and a smooth supershear transition. With over 4000 dynamic rupture simulations along faults separating similar and dissimilar materials, phase diagrams have been constructed to examine the conditions for the different transition mechanisms. The materials examined during the numerical simulations are the ones used in the laboratory experiments by Xia (2005), namely Homalite-100 and Polycarbonate as well as numerically derived 'intermediate materials'. For our simulations the generalized Rayleigh wave speed (Weertman 1963) exists and for all simulations separating dissimilar materials the bimaterial effect with normal stress changes around the rupture tip (Weertman 1980; Andrews & Ben-Zion 1997; Shi & Ben-Zion 2006) is present.

In a first step, the supershear transition mechanism for a fault separating similar materials is explored to benchmark against the analytical and numerical findings by Andrews (1976) and Xia *et al.* (2004), respectively. We found that the parameter S influences the occurrence of the supershear transition strongly as shown by Andrews (1976). The effect of rupture mode either being pulse-like or crack-like had only a very limited influence on the supershear transition mechanism when the velocity-weakening friction law of Ampuero & Ben-Zion (2008) is used. Two transition mechanisms were found for a fault separating similar materials, first the Burridge–Andrews mechanism (Burridge 1973; Andrews 1976) and secondly an unresolved supershear transition mechanism, which is seemingly smooth, but not to be mistaken for the smooth transition mechanism observed in the bimaterial experiments. The unresolved transition originates in the fact, that in a subshear velocity regime the crack tip travels at or below the Rayleigh wave speed (Rayleigh 1885) which is 94 per cent of the shear wave speed for the materials used here. When the transition length is small, the mesh resolution is not fine enough to show a secondary crack at the shear stress peak during transitioning, as the Rayleigh and shear wave speeds are very similar. This is different from other descriptions of smooth supershear transitions in the literature. Lu *et al.* (2009) observed a smooth transition at the original crack tip when a shear stress peak existed ahead of the rupture tip. The supershear transition was controlled by properties of their nucleation mechanism where normal stress was reduced at the nucleation site for a predefined time. The smooth transition shown here is also different from Festa & Vilotte (2006) where they have distinct shear waves travelling in front of the rupture tip when a smooth transition occurs.

During simulations of dynamic rupture along faults separating dissimilar materials, a third supershear transition mechanism was found: a smooth supershear transition. Rosakis (2002) suggested that explanations for a smooth supershear transition can be found by numerical modelling and in this study we showed that the bimaterial effect introduced by the material contrast across the interface promotes yielding in the negative direction where reduced normal stresses in front of the rupture unclamp the fault making it easier for the shear wave stress peak to trigger supershear failure of the fault. This is in agreement with Cochard & Rice (2000), Adams (2001), Ranjith & Rice (2001) and Shi & Ben-Zion (2006) who did not mention supershear transitions, but supershear propagation in the negative direction. In this direction, the normal stress is reduced across the interface ahead of the crack tip and promotes yielding of the fault in the vicinity of the crack tip. As the normal stress reduction is strongest along the fault between rupture tip and shear stress peak, a smeared out region ahead of the rupture tip yields simultaneously and accelerates the rupture tip to supershear speed. Once the rupture speed is supershear the entire bimaterial effect is located behind the crack tip and the normal stress change immediately after the crack tip is not compressional, but extensional as shown in Fig. 4 for $\Delta t = 71\,\mu$s and by Shi & Ben-Zion (2006). In the direction of slip of the more compliant material (positive direction) no smooth supershear transition is observed. Supershear transition occurs with the Burridge–Andrews mechanism or the unresolved supershear mechanism in the positive direction. The normal stress change is compressional across the interface ahead of the rupture tip in the positive direction (Andrews & Ben-Zion 1997, Fig. 7) and prevents or delays yielding of the material at the shear stress peak.

Phase diagrams are constructed from parameter sweeps (Fig. 5) which can be used to derive the following general statements.

(i) Higher material contrasts yield shorter transition lengths in the negative direction and larger transition lengths in the positive direction, as the normal stress reduction ahead of the rupture tip in the negative direction promotes earlier transitioning and the normal stress increase in the positive direction increases the transiton length.

(ii) If a material contrast across the fault exists, the supershear transition length is always shorter in the negative than in the positive direction.

(iii) If a supershear transition in the positive direction is present, there is also always a supershear transition present in the negative direction.

(iv) For a low parameter S, the transition mechanism is unresolved in both directions with the mesh sizes employed in this study.

(v) If the Burridge–Andrews mechanism is present in the negative direction for low material contrast, then for the same parameter S, but higher material contrast, the smooth supershear transition mechanism is present. Higher material contrast causes a stronger bimaterial effect and promotes the smooth supershear transition.

(vi) For a subset of simulations there was only a supershear transition in the negative direction, but none in the positive direction present. For short transition lengths, this is equivalent to the experimental results of Xia *et al.* (2005, case 2), for large transition lengths and a smooth transition mechanism it is equivalent to Xia *et al.* (2005, case 3).

(vii) For a given parameter S pulse-like ruptures have a larger supershear transition length than crack-like ruptures. This suggests, that the maximum parameter S, for which a supershear transition may occur, is lower for pulse-like than for crack-like rupture as shown in Dunham (2007, fig. 2). However, the length of the fault in the model used here, makes it difficult to access this part of the parameter space.

In our last parameter sweep, the influence of regularization of the effective normal stress on the transition mechanism is observed. Regularization has been proposed by Cochard & Rice (2000) to overcome the ill-posedness of two sliding bodies with dissimilar elastic properties (Renardy 1992; Ranjith & Rice 2001) with an existing generalized Rayleigh wave speed (Weertman 1963). As Cochard & Rice (2000) state, regularization leads to a different physical problem. In the studies presented here the normal stress changes are delayed and less pronounced when using the approach of Rubin & Ampuero (2007) and Ampuero & Ben-Zion (2008). This paper shows that with regularization the Burridge–Andrews mechanism occurs more readily also for higher material contrasts. For strong material contrast, however, the smooth transition is still observed. Regularization also changes transition lengths towards values observed in homogeneous cases.

Evidence is found that supershear transitions are possible in the positive direction and that large earthquakes can occur in both directions along a bimaterial fault. Another important finding is that supershear transitions along faults separating dissimilar materials occur for higher values of Andrews' parameter S than for faults separating similar materials. This means that earthquakes can become supershear for lower shear stresses along the fault than known from studies of faults separating similar materials. This, however, is only possible in the negative direction and it is due to the normal stress reduction ahead of the fault tip which promotes yielding. Thus, when observing a fault to estimate the likeliness of a supershear transition one must take into account material contrast.

7 CONCLUSIONS

The work presented here shows that the bimaterial effect can force supershear transitions to be smooth instead of following the Burridge–Andrews mechanism. This newly found smooth supershear transition mechanism in the negative direction is described in detail and reconfirms past experimental observations. If the material contrast along a bimaterial interface is high, supershear transitions in the direction of slip of the stiffer material occur for higher values of Andrews' parameter S than in the case of homogeneous materials. This is caused by the bimaterial effect promoting yielding of material ahead of the crack tip by lowered normal stress. The higher the material contrast, the more likely it is that a smooth transition occurs. In the direction of slip of the more compliant material, a smooth supershear transition exists exclusively due to a numerical effect for low values of parameter S and does not result from material contrast.

ACKNOWLEDGMENTS

We thank Aurelie Papon and Yaron Finzi for discussions and suggestions and we thank the reviewers Steven Day and Eric Dunham for constructive comments. This research is supported by The University of Queensland, the Australian Research Council Linkage project LP0562686 with the Queensland Department of Main Roads and The University of Queensland, and AuScope Ltd which is funded under the National Collaborative Research Infrastructure Strategy (NCRIS) an Australian Commonwealth Government Programme. Software was developed by the Australian Computational Earth Systems Simulator Major National Research Facility and computations were performed on the Australian Earth Systems Simulator, an SGI ICE 8200 EX supercomputer.

REFERENCES

Adams, G.G., 2001. An intersonic slip pulse at a frictional interface between dissimilar materials, *J. appl. Mech.,* **68**(1), 81–86.

Ampuero, J.-P. & Ben-Zion, Y., 2008. Cracks, pulses and macroscopic asymmetry of dynamic rupture on a bimaterial interface with velocity-weakening friction, *Geophys. J. Int.,* **173**(2), 674–692.

Andrews, D.J., 1976. Rupture velocity of plane strain shear cracks, *J. geophys. Res.,* **81**(32), 5679–5687.

Andrews, D.J., 1999. Test of two methods for faulting in finite difference calculations, *Bull. seism. Soc. Am.,* **89,** 931–937.

Andrews, D.J. & Ben-Zion, Y., 1997. Wrinkle-like slip pulse on a fault between different materials, *J. geophys. Res.,* **102,** 553–571.

Ben-Zion, Y., 2001. Dynamic ruptures in recent models of earthquake faults, *J. Mech. Phys. Solids,* **49,** 2209–2244.

Bouchon, M. & Vallée, M., 2003. Observation of long supershear rupture during the magnitude 8.1 kunlunshan earthquake., *Science,* **301**(5634), 824–826.

Burridge, R., 1973. Admissible speeds for plane-strain self-similar shear cracks with friction but lacking cohesion, *Geophys. J. Int.,* **35**(4), 439–455. doi:10.1111/j.1365-246X.1973.tb00608.x

Burridge, R., Conn, G. & Freund, L.B., 1979. The stability of a rapid mode ii shear crack with finite cohesive traction, *J. geophys. Res.,* **84,** 2210–2222.

Cochard, A. & Rice, J.R., 2000. Fault rupture between dissimilar materials: ill-posedness, regularization, and slip-pulse response, *J. geophys. Res.,* **105,** B11, doi:10.1029/2000JB900230

Das, S. & Aki, K., 1977. Fault plane with barriers: a versatile earthquake mode, *J. geophys. Res.,* **82,** 5658–5670.

Day, S.M., Dalguer, L.A., Lapusta, N. & Liu, Y., 2005. Comparison of finite difference and boundary integral solutions to three-dimensional

spontaneous rupture, *J. geophys. Res.,* **110,** B12307, doi:10.1029/2005JB003813.

Duan, B. & Oglesby, D.D., 2005. Multicycle dynamics of nonplanar strike-slip faults, *J. geophys. Res.,* **110,** B03304, doi:10.1029/2004JB003298.

Dunham, E.M., 2007. Conditions governing the occurrence of supershear ruptures under slip-weakening friction, *J. geophys. Res.,* **112,** B07302, doi:10.1029/2006JB004717.

Dunham, E.M. & Archuleta, R.J., 2004. Evidence for a supershear transient during the 2002 Denali fault earthquake, *Bull. seism. Soc. Am.,* **94**(6B), S256–S268.

Eshelby, J.D., 1949. Uniformly moving dislocations, *Proc. Phys. Soc. Sect. A,* **62**(5), 307–314.

Festa, G. & Vilotte, J.P., 2006. Influence of the rupture initiation on the intersonic transition: crack-like versus pulse-like modes, *Geophys. Res. Lett.,* **33,** L15320, doi:10.1029/2006GL026378.

Geuzaine, C. & Remacle, J.-F., 2009. GMSH: a 3-D finite element mesh generator with built-in pre- and post-processing facilities, *Int. J. Numer. Meth. Eng.,* **79**(11), 1309–1331.

Gross, L., Bourgouin, L., Hale, A.J. & Muhlhaus, H.B., 2007. Interface modeling in incompressible media using level sets in eScript, *Phys. Earth planet. Inter.,* **163,** 23–34.

Harris, R.A. & Day, S.M., 1993. Dynamics of fault interaction: parallel strike-slip faults, *J. geophys. Res.,* **98**(B3), 4461–4472.

Harris, R.A. & Day, S.M., 1997. Effects of a low-velocity zone on a dynamic rupture, *Bull. seism. Soc. Am.,* **87,** 1267–1280.

Langer, S., Olsen-Kettle, L.M., Weatherley, D.K., Gross, L. & Mühlhaus, H.-B., 2010. Numerical studies of quasi-static tectonic loading and dynamic rupture of bi-material interfaces, *Concurrency Computat. Pract. Exper.,* **22**(12), 1684–1702.

Langer, S., Weatherley, D. & Olsen-Kettle, L., 2011. Heterogeneities in earthquake rupture experiments with material contrasts, *J. Mech. Phys. Solids*, submitted.

Laursen, T.A. & Simo, J.C., 1993. A continuum-based finite element formulation for the implicit solution of multibody large deformation frictional contact problems, *Int. J. Numer. Meth. Eng.,* **36,** 3451–3485.

Lu, X., Lapusta, N. & Rosakis, A.J., 2009. Analysis of supershear transition regimes in rupture experiments: the effect of nucleation conditions and friction parameters, *Geophys. J. Int.,* **177**(2), 717–732, doi:10.1111/j.1365-246X.2009.04091.x

Mello, M., Bhat, H.S., Rosakis, A.J. & Kanamori, H., 2010. Identifying the unique ground motion signatures of supershear earthquakes: theory and experiments, *Tectonophysics,* **494,** 297–326.

Olsen-Kettle, L.M., Weatherley, D., Saez, E., Gross, L., Mühlhaus, H.B. & Xing, H.L., 2008. Analysis of slip-weakening frictional laws with static restrengthening and their implications on the scaling, asymmetry, and mode of dynamic rupture on homogeneous and bimaterial interfaces, *J. geophys. Res.,* **113,** B08307, doi:10.1029/2007JB005454

Perić, D. & Owen, D. R.J., 1992. Computational model for 3-D contact problems with friction based on the penalty method, *Int. J. Numer. Meth. Eng.,* **35,** 1289–1309.

Ranjith, K. & Rice, J.R., 2001. Slip dynamics at an interface between dissimilar materials, *J. Mech. Phys. Solids,* **49,** 341–361.

Rayleigh, J. W.S., 1885. On waves propagated along the plane surface of an elastic solid, *Proc. Lond. Math. Soc.,* **17**(1), 4–11.

Renardy, M., 1992. Ill-posedness at the boundary for elastic solids sliding under coulomb friction, *J. Elast.,* **27**(3), 281–287.

Rojas, O., Day, S., Castillo, J. & Dalguer, L.A., 2008. Modeling of rupture propagation using high-order mimetic finite differences, *Geophys. J. Int.,* **172,** 631–650.

Rosakis, A., Samudrala, O., Singh, R. & Shukla, A., 1998. Intersonic crack propagation in bimaterial systems, *J. Mech. Phys. Solids,* **46**(10), 1789–1814, doi:10.1016/S0022-5096(98)00036-2.

Rosakis, A.J., 2002. Intersonic shear cracks and fault ruptures, *Adv. Phys.,* **51**(4), 1189–1257, doi:10.1080/00018730210122328.

Rosakis, A.J., Xia, K., Lykotrafitis, G. & Kanamori, H., 2007. Dynamic shear rupture in frictional interfaces: speeds, directionality, and modes, in *Treatise on Geophysics,* pp. 153–192, ed. Schubert, G., Elsevier, Amsterdam.

Rubin, A.M. & Ampuero, J.-P., 2007. Aftershock asymmetry on a bimaterial interface, *J. geophys. Res.,* **112,** 0148–0227.

Shi, Z. & Ben-Zion, Y., 2006. Dynamic rupture on a bimaterial interface governed by slip-weakening friction, *Geophys. J. Int.,* **165**(2), 469–484, doi:10.1111/j.1365-246X.2006.02853.x.

Shi, Z., Ben-Zion, Y. & Needleman, A., 2008. Properties of dynamic rupture and energy partition in a solid with a frictional interface, *J. Mech. Phys. Solids,* **56**(1), 5–24, doi:10.1016/j.jmps.2007.04.006.

Singh, R.P. & Shukla, A., 1996. Subsonic and intersonic crack growth along a bimaterial interface, *J. appl. Mech.,* **63**(4), 919–924, doi:10.1115/1.2787247.

Stoneley, R., 1924. Elastic waves at the surface of separation of two solids, *Proc. R. Soc. Lond. Ser. A,* **106**(738), 416–428.

Wang, D. & Mori, J., 2012. The 2010 Qinghai, China, earthquake: a moderate earthquake with supershear rupture, *Bull. seism. Soc. Am.,* **102**(1), 301–308.

Weertman, J., 1963. Dislocations moving uniformly on the interface between isotropic media of different elastic properties, *J. Mech. Phys. Solids,* **11**(3), 197–204.

Weertman, J., 1980. Unstable slippage across a fault that separates elastic media of different elastic constants, *J. geophys. Res.,* **85**(B3), 1455–1461.

Weertman, J., 2002. Subsonic type earthquake dislocation moving at approximately $\sqrt{2}$ × shear wave velocity on interface between half spaces of slightly different elastic constants, *Geophys. Res. Lett.,* **29**(10), 1470, doi:10.1029/2001GL013916.

Wriggers, P., 2006. *Computational Contact Mechanics,* 2nd edn, Springer-Verlag, Berlin.

Xia, K., 2005. Laboratory investigations of earthquake dynamics, *PhD thesis*, California Institute of Technology, Pasadena, CA.

Xia, K., Rosakis, A.J. & Kanamori, H., 2004. Laboratory earthquakes: the sub-rayleigh-to-supershear rupture transition, *Science,* **303**(5665), 1859–1861.

Xia, K., Rosakis, A.J., Kanamori, H. & Rice, J.R., 2005. Laboratory earthquakes along inhomogeneous faults: directionality and supershear, *Science,* **308,** 681–684.